MISSOURI S&T University of Science & Technology

CENTER FOR INFRASTRUCTURE ENGINEERING STUDIES

Application of Active Microwave Thermography for Inspection of Rehabilitated Cement-Based Structures – Final Report

by

Ali Foudazi[1], Mohammad Tayeb Ghasr[1], Kristen M. Donnell[1], and Lesley H. Sneed[2]

[1]Applied Microwave Nondestructive Testing Laboratory (*amntl*)
Department of Electrical and Computer Engineering
[2]Department of Civil, Architectural, and Environmental Engineering
Missouri University of Science and Technology

Missouri University of Science and Technology

CIES 15-01

Disclaimer

The mission of CIES is to provide leadership in research and education for solving society's problems affecting the nation's infrastructure systems. CIES is the primary conduit for communication among those on the Missouri S&T campus interested in infrastructure studies and provides coordination for collaborative efforts. CIES activities include interdisciplinary research and development with projects tailored to address needs of federal agencies, state agencies, and private industry as well as technology transfer and continuing/distance education to the engineering community and industry.

Center for Infrastructure Engineering Studies (CIES)
Missouri University of Science and Technology
223 Engineering Research Lab
500 West 16th Street
Rolla, MO 65409-0710
Tel: (573) 341-4497; fax -6215
E-mail: cies@mst.edu
www.cies.mst.edu

Application of Active Microwave Thermography for Inspection of Rehabilitated Cement-Based Structures – Final Report

Ali Foudazi[1], Mohammad Tayeb Ghasr[1], Kristen M. Donnell[1], and Lesley H. Sneed[2]

[1]Applied Microwave Nondestructive Testing Laboratory (*amntl*)
Department of Electrical and Computer Engineering
[2]Department of Civil, Architectural, and Environmental Engineering
Missouri University of Science and Technology

Submitted to:
Dr. Kamal Khayat, Director

Center for Infrastructure Engineering Studies
Missouri University of Science and Technology

Project Objective

The primary objective for this work is to develop a novel nondestructive testing and evaluation (NDT&E) method for rapid inspection of rehabilitated cement-based structures through the integration of microwave nondestructive testing (NDT) and thermography, herein referred to as Active Microwave Thermography, or AMT.

AMT Principles

Active Microwave Thermography is a fairly new nondestructive testing technique based on the integration of microwave NDT principles and infrared thermography. By using microwave energy to heat a structure of interest, the resulting surface thermal profile may be monitored via a thermal camera. In general, there are two mechanisms of heating that are possible with AMT. First, (direct) dielectric heating may take place. Dielectric (e.g., non-conducting) materials are defined by their relative (to free-space) complex dielectric properties, given as $\varepsilon_r = \varepsilon_r' - j\varepsilon_r''$. The real part (permittivity) represents the ability of the material to store microwave energy, while the imaginary part (loss factor) represents the ability of the material to absorb microwave energy. Another heating mechanism may occur if conductive materials are present in the structure under inspection. In this case, current will be induced on the conductive material when under microwave illumination. These currents can serve as secondary sources of heat excitation.

Previous work has shown AMT to have the potential for the detection of corroded reinforcing steel bars [1-2], as well as inspection of steel fiber distribution in cement-based materials [3], carbon-based composites [4], and detection of delaminations/disbonds in layered structures [5]. Building on the success of these preliminary works, this work focused on developing AMT for inspection of cement-based structures that have been rehabilitated with fiber reinforced polymer (FRP)-based composites. Two common types of FRP-based composites are considered; carbon-based, referred to as carbon fiber reinforced polymer (CFRP) composites, and glass-based, referred to as glass fiber reinforced polymer (GFRP) composites. From an electromagnetic perspective, structures rehabilitated with GFRP are much easier to interrogate, as GFRP materials are dielectric materials (i.e., not conductive), and hence the microwave excitation can easily penetrate through the GFRP. This is especially useful in the case of layered structures. Structures rehabilitated with CFRP are more challenging from an inspection point-of-view, as CFRP is conductive (due to the presence of the carbon), and therefore it is more difficult to penetrate beyond the first layer of CFRP. However, it is not impossible to inspect subsequent (beyond the first) layers. Polarization (i.e., orientation of the incident electric field) of the microwave excitation with respect to the CFRP fiber orientation (i.e., parallel or perpendicular to the fiber orientation) can be utilized to permit the microwave excitation to penetrate to subsequent layers. Another option is to take advantage of the induced current in the CFRP that may serve as a secondary heat source.

Simulations

To begin, a coupled microwave-thermal co-simulation is conducted using CST Microwave Studio® and MPHYSICS Studio®. The simulation is conducted in two parts; first, the electromagnetic response (i.e., electric and magnetic field inside dielectric materials and/or induced current on conducting surfaces) is determined. For these simulations, the excitation signal is a plane wave with 50 W power operating at a frequency of 2.4 GHz. From this, the transient thermal response is calculated (i.e., heat generation and diffusion during the heating period) based on the electromagnetic response. For this work, two cases are considered that include a layered structure of CFRP (Case 1) and GFRP (Case 2) bonded onto a concrete block (i.e., rehabilitated concrete using CFRP/GFRP). The rehabilitated samples include disbonds (i.e., air-filled voids) of various depths and sizes.

Case 1 – CFRP

The first structure considered for simulation is a concrete block with dimensions of 25 cm × 25 cm × 5 cm. The concrete block is rehabilitated with two layers of CFRP, as shown in Fig. 1. In addition, the presence of adhesive (between the two CFRP layers and between the internal CFRP layer and concrete) is included in this model. Thus, the structure is multi-layered consisting of the following layers: 1) concrete, 2) adhesive, 3) CFRP, 4) adhesive, 5) CFRP, 6) air, as shown in Fig. 2. The thickness of CFRP layer is 0.5 mm, and the thickness of adhesive is 0.5 mm. Also, the air layer is considered as an infinite half-space. It should be noted that this is a simplified model used for preliminary simulations. In practice the adhesive is mixed in with the fibers.

At the interface between layer 1 and 3 (concrete and CFRP), two locations in the adhesive layer (layer 2) are considered as having a lack of adhesive (i.e., a location where the internal CFRP layer has debonded from the concrete), each with different dimensions. In this case, a lack of adhesive is considered to be an air-filled void between the concrete and CFRP layers. In Fig. 1, they are shown as gray rectangles labeled as D1 and D2. At layer 4 (second adhesive layer), two additional portions with a lack of adhesive (i.e., air-filled void) are considered, where CFRP layers 3 and 5 have debonded from one another. In Fig. 1, these disbonds are shown as white rectangles labeled D3 and D4. In all cases, the larger disbonds have dimensions of 3 cm × 3 cm, and the smaller disbonds have dimensions of 2 cm × 2 cm. The center-to-center spacing between disbonds is 10 cm in order to minimally affect the heat diffusion of neighboring disbonds. Thus, it is assumed that the thermal response for each debonded portion is independent of nearby disbonds.

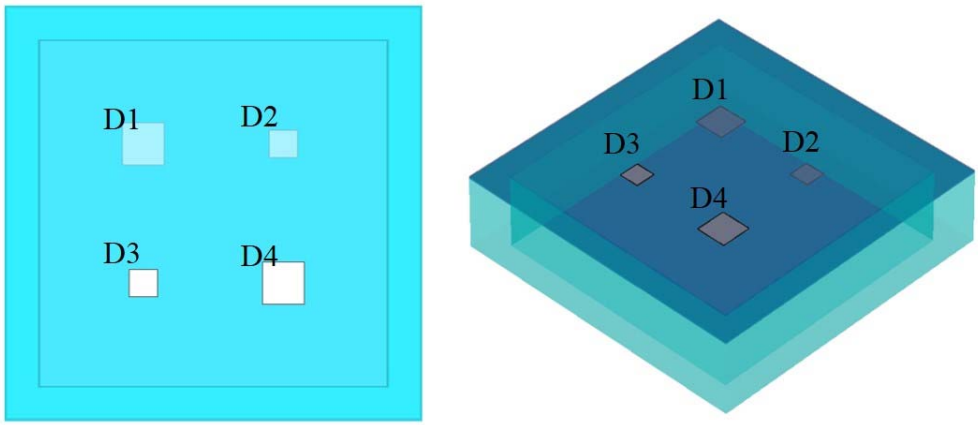

Fig 1- Top views of the sample.

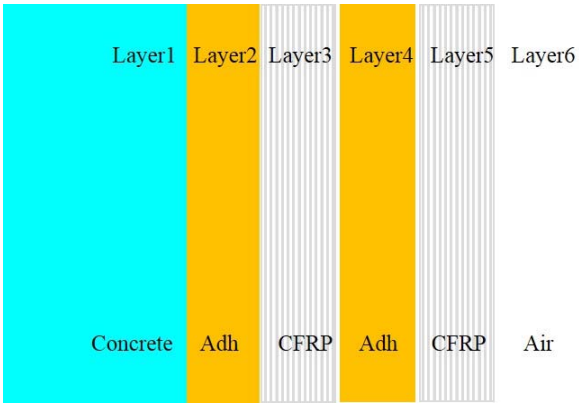

Fig 2- Side view of the sample.

The dielectric and thermal properties determine the induced heat and subsequent heat diffusion in any material. In Table I, the dielectric and thermal properties (necessary for simulation) of these four materials are provided. As discussed above, ε_r is a complex value in which the real part and imaginary parts are called permittivity and loss factor, respectively. Thus, as shown in Table I, air is a lossless dielectric material and adhesive and concrete are lossy dielectric materials. In addition, σ represents the electrical conductivity and indicates that CFRP is a decent electrical conductor. This is significant as it pertains to AMT as microwave energy cannot (in general) penetrate conductive media. As CFRP is the outer layer of structure and is an electrically conductive material, the heating mechanism in cement-based materials rehabilitated with CFRP under AMT inspection is due to the induced surface current on the CFRP. In addition and considering thermal properties, by comparing the thermal conductivity of air (0.026 W/m.K) and adhesive (1.0 W/m.K), air is considered to act as a thermal insulator between two layers, and the adhesive is considered to be a thermal conductor. Hence, it is expected that the debonded areas will experience higher temperatures than healthy areas when monitoring the surface of the sample and will therefore appear as hot spots in thermal images.

Table I – Dielectric and thermal properties of materials [1], [4], [5].

	Material (dielectric) Properties	Thermal Conductivity (W/m.K)	Specific Heat (KJ/Kg.K)	Density (Kg/m^3)	Diffusivity (m^2/s)
Air	$\varepsilon_r = 1$	0.026	1.005	1.204	21.5×10^{-6}
Concrete	$\varepsilon_r = 10\text{-}j4$	1.7	0.8	2400	0.88×10^{-6}
CFRP	$\sigma = 10^4$	0.8	1.2	1600	0.41×10^{-6}
Adhesive	$\varepsilon_r = 6\text{-}j0.6$	1.0	3.7	1100	0.24×10^{-6}

In order to show the temperature rise at different times, the temperature increase, ΔT, with respect to the temperature at the start of the microwave illumination ($t_0 = 0$ sec), is considered in order to remove the effect of background temperature, given by:

$$\Delta T(t) = T(t) - T(t_0) \qquad (1)$$

where $\Delta T(t)$ is the temperature increase at time t, $T(t)$ is the (absolute) temperature observed at time t, and $T(t_0)$ is the absolute temperature at time t_0. In Fig. 3a and b, the surface temperature increase for each debonded area as well as an arbitrary non-debonded (healthy) point that serves as a reference point are shown. For this case, the sample is illuminated for 1000 sec with microwave energy, and the heat diffusion is monitored during this same time. From Fig. 3a, it is seen that the reference point (R), located in the middle of the sample at a healthy (no disbonds) location, has a linear response when viewed in a logarithmic scale. Moreover, the surface temperature of the debonded areas deviates from the reference line at a specific time which is related to the depth of disbond. More specifically, disbonds D1and D2 are farther from the surface than disbonds D3 and D4. Hence, the amount of time that is required for heat diffusion (to the surface where it can be detected) is longer for disbonds D1 and D2 than D3 and D4, and therefore the deviation from the reference line occurs later for D1 and D2. This is important as the location of the disbond may be determined from the surface temperature. Also, it can be seen that for two debonded areas with the same depth, e.g., D1 and D2, the temperature rise experiences a second breaking point that is related to disbond size. This is quite important as this indicates the potential for feature extraction from the thermal response when viewed

on a logarithmic scale. It is also interesting to note that when viewed in a linear scale (Fig. 3b), the effect of disbond location is not obvious from non-debonded area (i.e., the reference point).

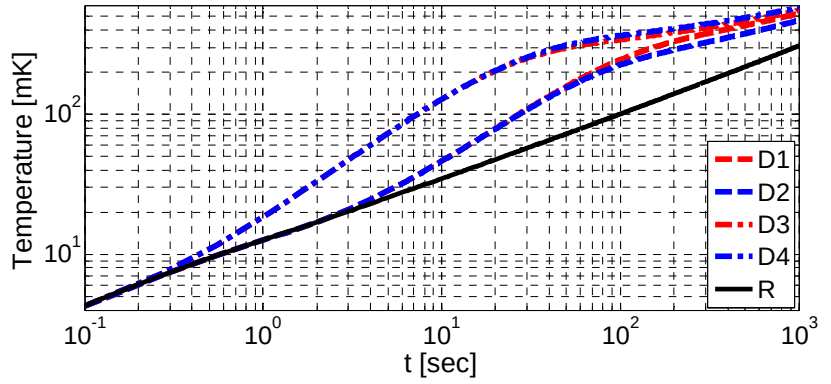

(a)

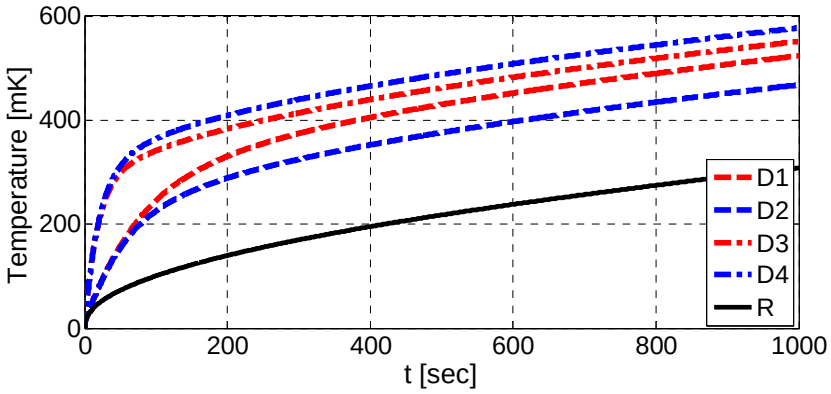

(b)

Fig 3- Temperature variation for different disbonds and reference point (a) logarithmic scale, (b) linear scale, for rehabilitation with CFRP.

In order to better analyze the results of Fig. 3a, a "zoomed in" view (at the point of deviation from the reference) is presented in Fig. 4. In Fig. 4a, the first breaking point from the reference point is presented. As discussed above, because D3 and D4 are closer to the surface of the sample, the first breaking point (i.e., deviation from R) occurs sooner in time (~ t = 0.5 sec) than that of the two other disbonds (D1 and D2) in time (~ t = 3.5 sec). The deviation from the reference point is an indication of presence of air (i.e., thermal insulation). In addition, it can be concluded that while D1 and D2 have the same depth but different dimensions, the first breaking point is independent of disbond size and is only related to the depth of disbond from the surface. Moreover in Fig. 4b and Fig. 4c, the second breaking points are presented. From Fig. 4b, D1 and D2 experience a second breaking point at ~ t = 60 sec, while from Fig. 4c, the second breaking point for D3 and D4 occurs at ~ t = 30 sec. This is significant in that the second breaking point shows the deviation in thermal response between two debonded portions (of different dimensions) with the same disbond depth. It is seen that the larger disbond for a given depth from the surface (i.e., D1 > D2 and D4 > D3) experiences a higher temperature after the second break point.

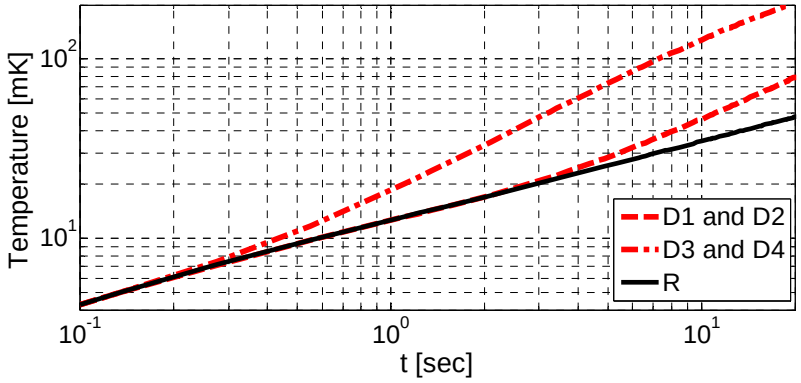

(a)

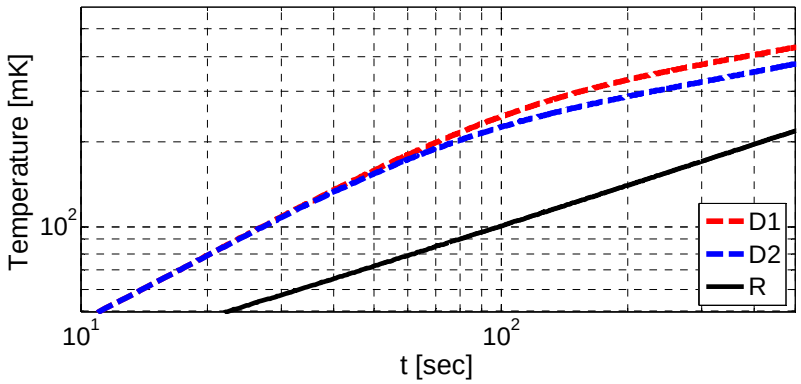

(b)

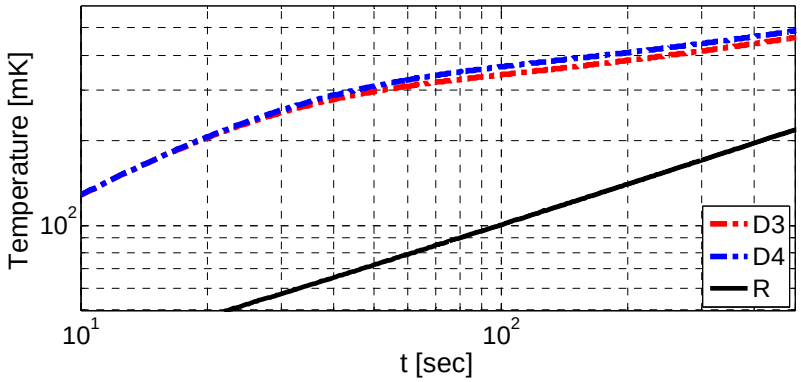

(c)

Fig 4- Breaking point indication in logarithmic scale.

In addition, to show the difference between disbond size and depth, the temperature profile at the surface of the sample after 0.5, 3.5, 30 and 60 sec (i.e., related to the breaking point discussion above) is provided in Fig. 5. These thermal images of the surface of the sample confirm that since the debonded area (i.e., air-filled void) has a lower thermal conductivity than the healthy area (i.e., with adhesive, see Table I), debonded areas are seen as hot spots in the thermal profile. Also, disbonds closer to the surface (D3 and D4) have a higher temperature (and thus appear brighter) than those located farther away (D1 and D2).

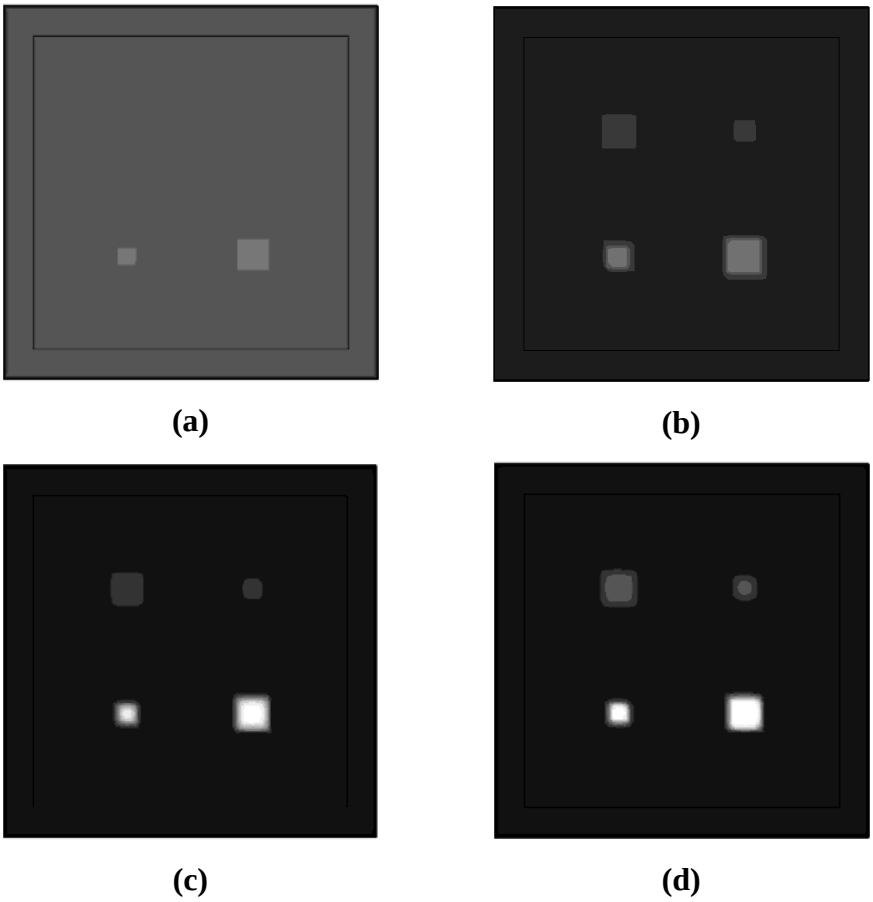

Fig 5- Temperature profile view after (a) 0.5, (b) 3.5, (c) 30, and (d) 60 sec of heating.

Case 2 - GFRP

In this case, two layers of GFRP are considered, with the sample configuration identical to that of Case 1 (CFRP) above, with the CFRP layers now replaced with GFRP layers. The only difference in this case is that GPRF is a dielectric while CFRP (from above) is conductive. As such, since GFRP and adhesive are lossy dielectric materials, dielectric heating takes place. In Table II, the dielectric and thermal properties of the materials used for rehabilitated cement-based structure with GFRP are provided.

Table II- Dielectric and thermal properties of materials.

	Dielectric Properties	Thermal Conductivity (W/m.K)	Specific Heat (KJ/Kg.K)	Density (Kg/m^3)	Diffusivity (m^2/s)
Air	$\varepsilon_r = 1$	0.026	1.005	1.204	21.5×10^{-6}
Concrete	$\varepsilon_r = 10\text{-}j4$	1.7	0.8	2400	0.88×10^{-6}
GFRP	$\varepsilon_r = 4.1\text{-}j0.08$	1	0.807	2550	0.48×10^{-6}
Adhesive	$\varepsilon_r = 6\text{-}j0.6$	1	3.7	1100	0.24×10^{-6}

From the surface temperature results shown in Fig. 6, it is seen that the healthy area has a higher temperature than the debonded portion. As such, it can be concluded that when using AMT to inspect GFRP-based structures, disbonds present as cold (or cooler than the surrounding material) spots. However, information regarding disbond depth is not available from the results of Fig. 6. As such, further modeling and simulation for rehabilitated concrete with GFRP is required and is ongoing. Also, feature extraction based on the logarithmic scale analysis also needs to be investigated.

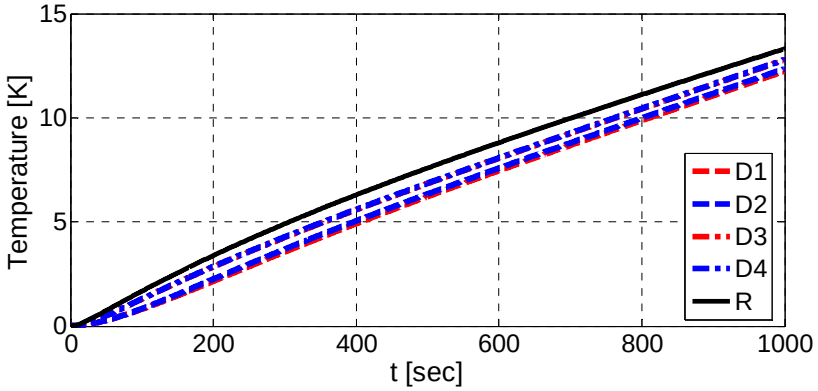

Fig 6- Temperature variation for disbonds and reference point.

Measurements

To further support AMT as a potential NDT&E tool for rapid inspection of rehabilitated cement-based structures, measurements were conducted on a concrete block with a two-layer CFRP laminate applied to the surface. Both perpendicular and parallel polarization (with respect to the fiber orientation) of the illuminating microwave energy were utilized for these measurements.

The general measurement schematic is shown in Fig. 7a. The block (made of mortar) has dimensions of 52 cm × 38 cm × 9 cm, and the two layers of CFRP bonded to the mortar surface consist of unidirectional fibers (the fibers of both layers were oriented in the same direction). The block includes a debonded area made by placing a thin sheet of foam, which can be considered (electromagnetically and thermally) to be the equivalent to air, between the CFRP laminate and mortar with dimensions of 6 cm × 8 cm. Generally, the thermal conductivity of foam as an insulator is 0.03 W/m.K, which is very close to air with a thermal conductivity of 0.026 W/m.K. Also, the specific heat of foam and air is 1.3 and 1.005 KJ/Kg.K, respectively (and are also very similar). Moreover, dielectric properties of foam are very similar to air. Thus, the artificial disbonds created using foam are considered to be similar to those occurring in practice. The debonded portion is located in the center part of the block face to reduce the effect of the sides (edges) on the diffusion of heat at the debonded areas.

The measurements were conducted using an AMT system including a signal generator that produced sinusoidal excitation amplified to a power level of 50 W of microwave energy at a frequency of 2.4 GHz that was transmitted using a TEM horn antenna (dimensions of 14 cm × 24 cm). The distance between the antenna and sample (i.e., liftoff) was 20 cm (i.e., a sufficient distance to permit an inspection of a majority of the surface area of the sample), as is shown in Fig. 7b. To acquire thermal images, an infrared camera, DRS320, with a sensitivity of 50 mK is utilized. The images are acquired by using an image acquisition unit and recorded for post-processing. The rate of image acquisition is 30 frames per second. Therefore, by using the averaged value of 30 frames together for each time step of 1 sec, the detection sensitivity obtained

during post-processing may approach a much lower value than the initial sensitivity of the camera. A PC is used to synchronize the signal generator, amplifier, thermal camera and image acquisition unit together.

The set-up shown here illustrates the antenna orientation used for a perpendicular polarization illumination. In this case, the angle between electric field radiated toward the sample with the fibers orientation is 90 degrees. For parallel polarization, the sample will rotate 90 degrees and electric field and fiber orientation will be oriented in the same direction. After post-processing, the results for parallel polarization are shown in Fig. 8 and Fig. 9, and in Fig. 10-12 for perpendicular polarization. Also, a comparison of the temperature rise between both polarizations is provided in Fig. 13.

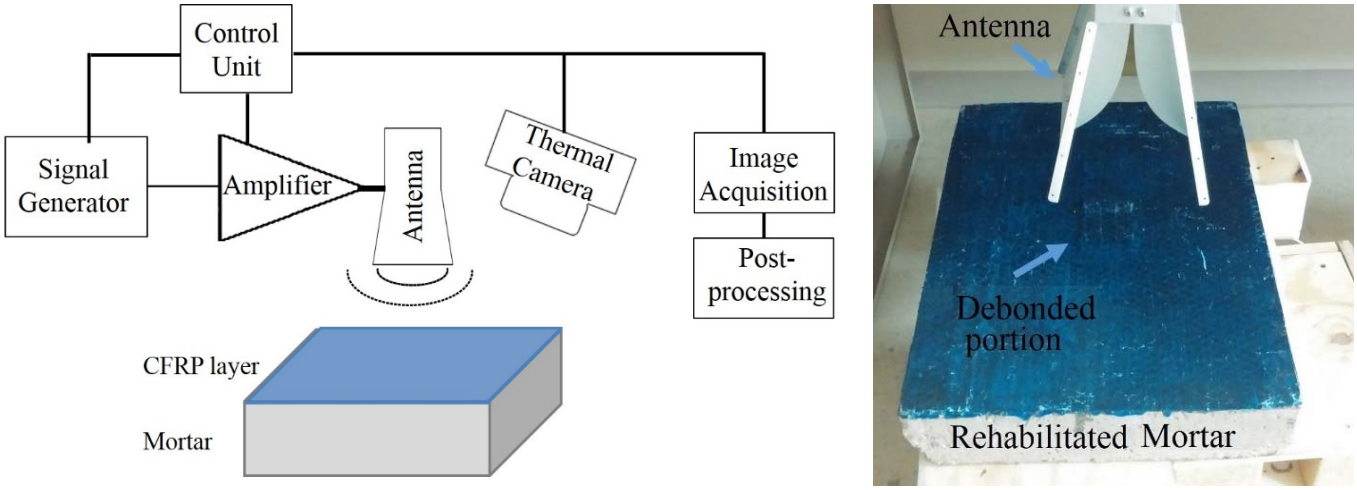

(a) **(b)**

Fig 7- (a) AMT measurement schematic, (b) measurement set-up for perpendicular polarization of applied microwave energy with respect to the fiber orientation.

Case 1: Parallel Polarization

By heating the sample via a microwave excitation and as mentioned above, it is expected that the debonded portion (i.e., a thin sheet of foam inserted between the mortar and CFRP layer instead of air-filled void) will appear as a hot spot in the thermal image due to the lower thermal conductivity of air (compared to that of adhesive). As shown in Fig. 8 for the thermal images after t = 30, 60, 90, and 120 sec heating, it is seen that the debonded area after 30 sec of microwave excitation may not be detected in the case of a noisy environment since the temperature change is very small (~ 5 mK) and may not be measurable, as typical commercially available thermal cameras have a sensitivity on the order of 50 mK (even after post-processing). Thus, for this case, heating for a longer period of time may alleviate this concern. To illustrate this, the results after t = 60 sec of microwave excitation show that the temperature of the debonded area has increased (to a measurable difference of ~ 10 mK), while the temperature of the rest of the sample has essentially remained constant. A similar response can be seen at 90 sec and 120 sec, where the debonded area is evident, and the temperature of the surrounding mortar remains constant (although has increased from that of lesser heat times). Next in Fig. 9, the results of heating after t = 200 sec, including a cross-sectional view of the temperature difference across the debonded area, are presented.

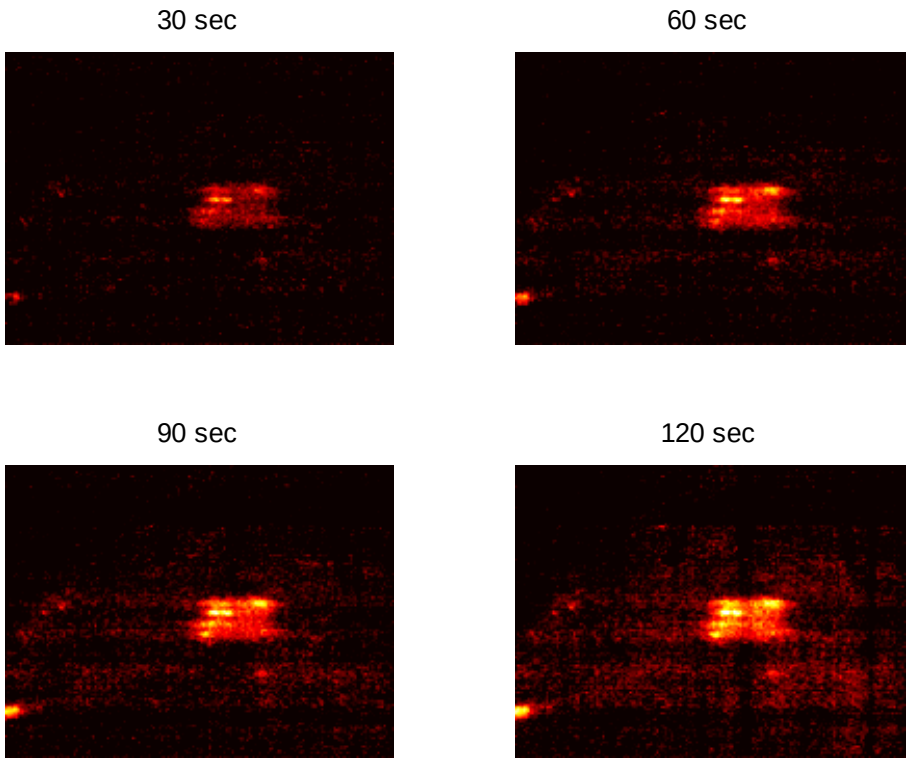

Fig 8- Thermal images for parallel polarization after t = 30, 60, 90, and 120 sec.

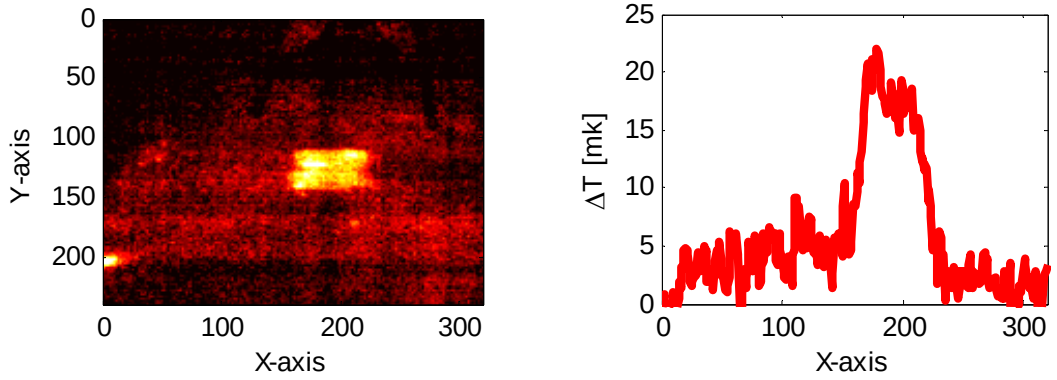

(a) **(b)**

Fig 9- Measurement results of parallel polarization at t = 200 sec, (a) thermal image, and (b) cross sectional view of temperature across debonded area.

From the results in Fig. 9a, the debonded portion appears as a hot spot with overall temperature of ~ 20 mK, and the rest of the area heats up slightly with average value of ~ 4 mK across the surface of the sample. The presence of a hot spot is due to the differences in thermal properties of adhesive and air (or foam). Also from Fig. 9b, when considering the change in temperature (from a healthy area) across a line that is parallel to the x-axis and includes debonded area, the temperature profile appears similar to a pulse with a very small (~ 4 mK) value for healthy areas, and has a sharp increases at the edge of the debonded area. Moreover, the magnitude of this temperature rise (i.e., ~ 20 mK at average) is related to the power level of the incident microwave energy, liftoff, direction of polarization, thermal properties of mortar, CFRP,

adhesive, and air, etc. In addition, the width of the pulse is related to the width of the disbond. Further, it can also be seen that at that debonded area, the temperature at the left edge (~ 23 mK) of the disbond is greater than that of the right edge (~ 18 mK). This may indicate that the disbond is larger on the left side, or may be due to measurement error (as the temperature difference here is quite small between two sides, ~ 5 mK). These results also indicate that even after 200 sec of microwave illumination, the temperature increase at the disband is only 20 mK (which may not be sufficient for reliable detection). As such, in the next section, the effect of perpendicular polarization for disbond detection is presented and discussed.

Case 2: Perpendicular Polarization

Similar to the previous case (parallel polarization), it is expected that when the fiber orientation is perpendicular to the polarization of the microwave excitation, the debonded portion will appear as a hot spot in the middle of the thermal image. However, an important difference between this case and the previous is that now, the microwave energy that can penetrate through the CFRP fibers (essentially by passing through the space between fibers), thus leading to dielectric heating (which was not possible for a parallel polarization excitation). The thermal image results for this excitation are shown below in Fig. 10.

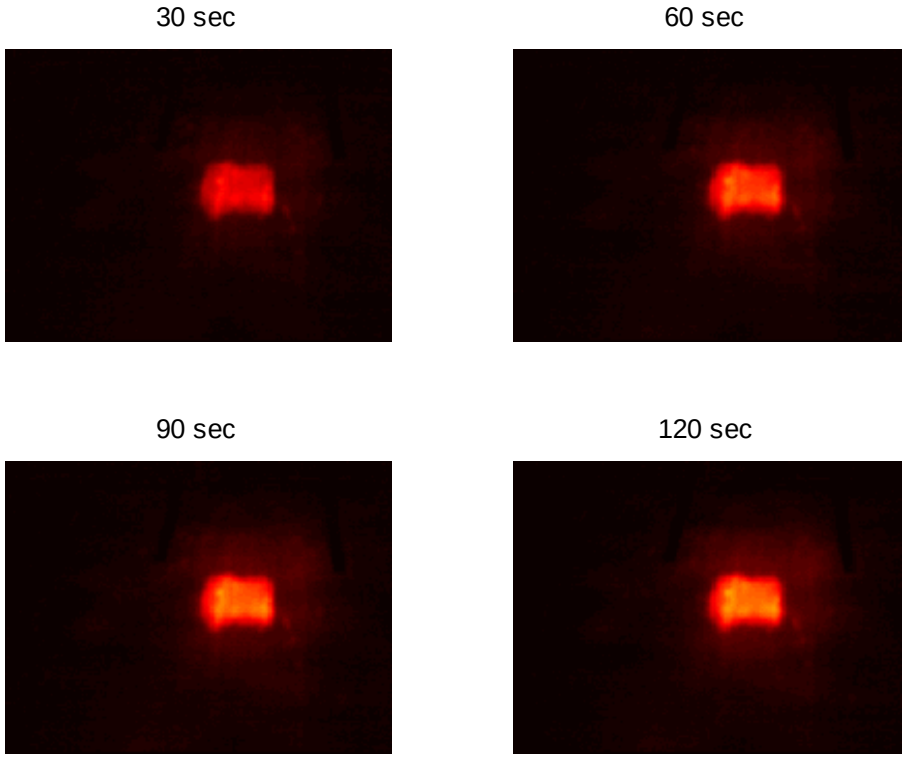

Fig 10- Thermal images for perpendicular polarization after t = 30, 60, 90, and 120 sec.

In Fig. 10, the surface thermal profile of the rehabilitated mortar with CFRP is shown for perpendicular polarization after t = 30, 60, 90 and 120 sec of heating. For this case, the temperature at the debonded area is much higher (by ~ 180 mK) than the healthy area, even after 30 sec, thereby indicating the ability of AMT to detect the debonded area faster (and more reliable) than the parallel polarization case. The temperature at the debonded area increases to ~ 205, ~ 220 and ~ 230 mK after 60, 90 and 120 sec heating, respectively. While the position of the camera and antenna were fixed for measurements of both cases, the sample was rotated counter clockwise to change from the parallel to the perpendicular polarization case.

Hence, the bottom edge of the debonded area in Fig. 10 corresponds to the left edge of the debonded area in Fig. 9b. From Fig. 10, it appears that that bottom part of the debonded area may have a higher temperature than its' top area. Thus, this supports the possibility that the bottom part of the debonded area may be larger than the top part. This result also confirms the temperature variation across the debonded area in Fig. 9b, in which the left side (for parallel polarization, the bottom side for perpendicular polarization) has a higher temperature than the right side (for parallel polarization, the top side for perpendicular polarization). To further illustrate the improvement offered by utilizing perpendicular polarization, a cross-sectional view of the temperature difference of the debonded area after 200 sec of heating is shown next in Fig. 11 along with a 3-dimensional view of the surface thermal profile is shown in Fig. 12 (to provide an alternate view of the results).

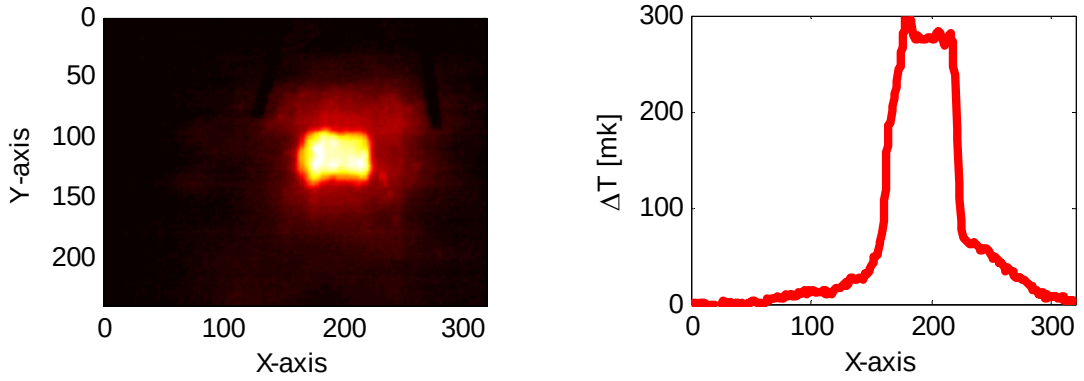

(a) **(b)**

Fig 11- Measurement results of perpendicular polarization at t = 200 sec, (a) thermal image, and (b) cross sectional view of temperature across debonded area.

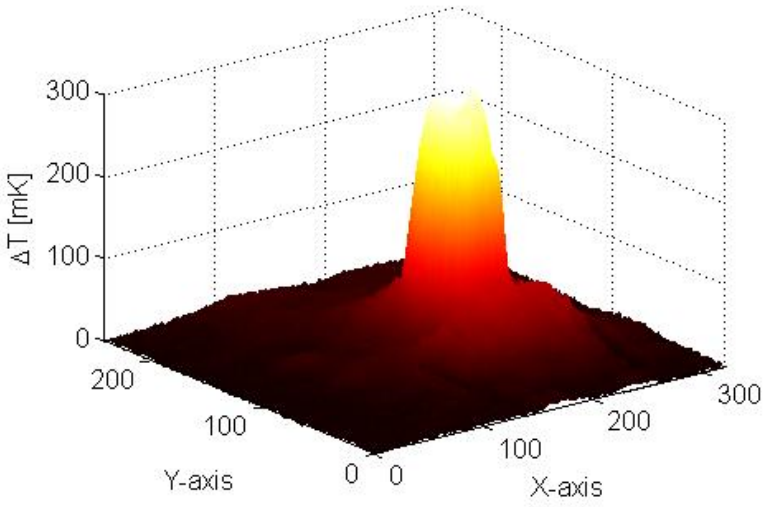

Fig 12- 3-D measurement results for perpendicular polarization at t = 200 sec.

From Fig. 11a, it is easy to see that the thermal image results after t = 200 sec of microwave excitation for perpendicular polarization depict a contrast between the debonded area and the healthy area. Moreover,

from Fig. 11b, when considering the change in temperature (from a healthy area) across a line that is parallel to the x-axis and includes debonded area, the temperature profile appears similar to a pulse with an average temperature variation of ~ 5 mK value for healthy areas, and increases over the debonded area with average temperature variation of ~ 280 mK. The difference between temperature at the healthy area and debonded area is well beyond the typical sensitivity of 50 mK and potential post-processing sensitivity of much lower than 50 mK and therefore easily measurable (and reliable). As above, the magnitude of this temperature increase is proportional to the power level of the incident microwave energy, liftoff, thermal properties of mortar, CFRP, adhesive and air, etc. The width of the pulse indicates the width of the disbond with respect to the position of camera and view angle (i.e., similar to previous measurement). Further, it can also be seen that at that debonded area, the temperature at the left edge (~ 300 mK) of the disbond is greater than that of the right edge (~ 285 mK). This may indicate that the disbond is larger on the left side in perpendicular polarization (i.e., top side in parallel polarization) as compared to the right side in perpendicular polarization (i.e., bottom side in parallel polarization). Since the results are larger than the post-processing sensitivity, it is believed that the indications of the disbond presented here are more likely (than those speculated in the parallel polarization results). This is an excellent example of illustrating the importance of heating a sample to a temperature change that is beyond the measurement sensitivity.

Effect of Polarization

As has been shown, polarization in AMT plays an important role for inspection of cement-based materials rehabilitated with CFRP. As discussed above, when the microwave excitation has parallel polarization, the heating mechanism is due to induced surface current on fibers, as the microwave energy cannot penetrate through the CFRP (and is reflected back). For perpendicular polarization, more of the energy passes through the CFRP into the underlying dielectric material (mortar) and therefore dielectric heating takes place. As such, it is not unexpected that the resulting induced heat may differ between the two polarization excitations. To this end, in Fig. 13, the temperature increase of the debonded area (with respect to the healthy area) is shown for both polarizations.

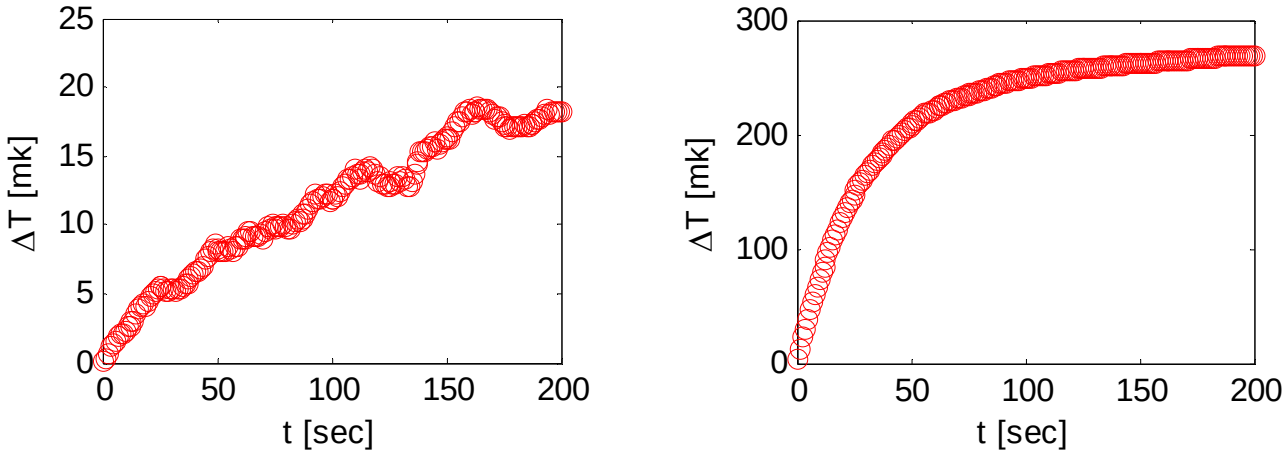

Fig 13- Temperature difference for (a) parallel, (b) perpendicular polarization irradiation.

From the results in Fig. 13, it is seen that the temperature increases from the initial temperature of 0 to 20 mK (for parallel polarization) and to 280 mK (for perpendicular polarization) after 200 sec of microwave illumination. Clearly, perpendicular polarization is a better choice in this case. However, the effect of

polarization on heat generation warrants further study since more energy penetrates into the (underlying) concrete sample under perpendicular polarization illumination but the temperature increase of the concrete is similar to when under parallel polarization illumination.

Additionally, small thermal variations are evident in Fig. 13a (parallel) that are not evident in Fig. 13b (perpendicular). These variations are attributed to measurement uncertainty, as the temperature increase for parallel polarization illumination is on the order of the sensitivity of thermal camera. As such, in order to make reliable AMT measurements, a longer heating time (or increased incident power) is required for parallel polarization than for perpendicular polarization. More importantly and from a practical standpoint, these results also indicate that in the case of bi-directional fiber layers (which are more common in practice), the results indicate that inspection via AMT is also possible (as this is essentially a case where both perpendicular and parallel excitation will be used), albeit with a potential increase in heat time and/or power requirements.

Conclusion

In this report, an investigation into the potential for AMT to serve as a nondestructive testing and evaluation method for rapid inspection of rehabilitated cement-based structures with CFRP/GFRP is presented. From the simulation results, the results show that AMT has the potential to locate disbonds between various layers of a layered structure when rehabilitated with CFRP. Measurement results show that when the CFRP fiber orientation is perpendicular to the illuminating microwave energy, the debonded area can be detected faster (or possibly with less power) than what is required to detect disbonds using parallel polarization. Inspection of GFRP-rehabilitated structures has not been successful thus far. Future work will include more in-depth studies on GFRP-based rehabilitated structures. Additionally, further study on the effect of polarization on heat generation is also necessary to further develop AMT for detection of disbonds/delaminations for carbon-based rehabilitations.

References

1. Foudazi, A., M.T. Ghasr, and K.M. Donnell, “Characterization of Corroded Reinforced Steel Bars by Active Microwave Thermography”, *accepted for publication in the IEEE Transactions on Instrumentation and Measurement.*
2. Pieper, D., K.M. Donnell, M.T. Ghasr, and E.C. Kinzel. "Integration of Microwave and Thermographic NDT Methods for Corrosion Detection" *Proceedings of the 40th Annual Review of Progress in Quantitative Nondestructive Evaluation Conference, American Institute of Physics, Conference Proceedings 1581*, pp. 1560-1567. AIP Publishing, 2014.
3. Foudazi, A., I. Mehdipour, K.M. Donnell, and K.H. Khayat, “Detection of Steel Fibers in Cement-based Materials by Active Microwave Thermography”, *Presented at the 14th International Symposium on Nondestructive Characterization of Materials (NDCM2015)*, Marina del Rey California, June 22-26, 2015.
4. Foudazi, A., M.T. Ghasr, and K.M. Donnell, “Application of Active Microwave Thermography to Inspection of Carbon Fiber Reinforced Composites”, *Proceedings of the 2014 IEEE AUTOTEST Conference,* Sept. 15-18, 2014, St. Louis, MO.
5. Foudazi, A., M.T. Ghasr, and K.M. Donnell, “Application of Active Microwave Thermography to Delamination Detection”, *Proceedings of the International Instrumentation and Measurement Technology Conference (I2MTC),* pp. 1567-1571, May 12-15, 2014, Montevideo, Uruguay.